Disentangling the multifactorial contributions of fibronectin, collagen and cyclic strain on MMP expression and extracellular matrix remodeling by fibroblasts

Matrix Biology 40 (2014) 62–72

Contents lists available at ScienceDirect

Matrix Biology

journal homepage: www.elsevier.com/locate/matbio

Disentangling the multifactorial contributions of fibronectin, collagen and cyclic strain on MMP expression and extracellular matrix remodeling by fibroblasts

Yang Zhang [a,1], Zhe Lin [a,1], Jasper Foolen [a], Ingmar Schoen [a], Alberto Santoro [a], Marcy Zenobi-Wong [b], Viola Vogel [a,*]

[a] Laboratory of Applied Mechanobiology, Department of Health Sciences and Technology, ETH Zurich, Vladimir-Prelog-Weg 4, CH-8093 Zurich, Switzerland
[b] Cartilage Engineering + Regeneration, Department of Health Sciences and Technology, ETH Zurich, Otto-Stern-Weg 7, CH-8093 Zurich, Switzerland

ARTICLE INFO

Article history:
Received 5 July 2014
Received in revised form 3 September 2014
Accepted 4 September 2014
Available online 11 September 2014

Keywords:
Mechanobiology
Human foreskin fibroblasts
Cyclic stretching
Matrix metalloproteinases
FRET-based molecular tension sensors

ABSTRACT

Early wound healing is associated with fibroblasts assembling a provisional fibronectin-rich extracellular matrix (ECM), which is subsequently remodeled and interlaced by type I collagen. This exposes fibroblasts to time-variant sets of matrices during different stages of wound healing. Our goal was thus to gain insight into the ECM-driven functional regulation of human foreskin fibroblasts (HFFs) being either anchored to a fibronectin (Fn) or to a collagen-decorated matrix, in the absence or presence of cyclic mechanical strain. While the cells reoriented in response to the onset of uniaxial cyclic strain, cells assembled exogenously added Fn with a preferential Fn-fiber alignment along their new orientation. Exposure of HFFs to exogenous Fn resulted in an increase in matrix metalloproteinase (MMP) expression levels, i.e. MMP-15 (RT-qPCR), and MMP-9 activity (zymography), while subsequent exposure to collagen slightly reduced MMP-15 expression and MMP-9 activity compared to Fn-exposure alone. Cyclic strain upregulated Fn fibrillogenesis and actin stress fiber formation, but had comparatively little effect on MMP activity. We thus propose that the appearance of collagen might start to steer HFFs towards homeostasis, as it decreased both MMP secretion and the tension of Fn matrix fibrils as assessed by Fluorescence Resonance Energy Transfer. These results suggest that HFFs might have a high ECM remodeling or repair capacity in contact with Fn alone (early event), which is reduced in the presence of Col1 (later event), thereby down-tuning HFF activity, a processes which would be required in a tissue repair process to finally reach tissue homeostasis.

1. Introduction

Fibroblasts are the most abundant cell type in connective tissues and are the primary cells that lay down the first provisional ECM that is rich in fibronectin (Fn) (Clark, 1990; Hynes, 2009; Shaw and Martin, 2009). During early wound healing, the provisional Fn-rich matrix is remodeled and later interlaced by type I collagen (Col1) and type III collagen (Reinke and Sorg, 2012), of which excessive bundling often leads to problematic fibrosis (Gabbiani, 2003; Shaw and Martin, 2009; Bryers et al., 2012) and excessive wound contracture (Montesano and Orci, 1988; da Rocha-Azevedo et al., 2013). Also mechanical forces acting on cells and tissues affect many physiological processes, from tissue development such as the assembly and remodeling of extracellular matrix (ECM) in connective tissue (Tomasek et al., 2002; Chiquet et al., 2009; Geiger et al., 2009; Cox and Erler, 2011; Dideriksen et al., 2013) to repair processes such as wound healing (Kippenberger et al., 2000; Gabbiani, 2003; Wong et al., 2011) and scar formation (Aarabi et al., 2007; Gurtner et al, 2008; Wong et al., 2012).

Disentangling the contributions of mechanical forces on cell functions, from those induced by altered ECM composition versus altered physical properties, as well as of changes in local MMP activity remains a challenge, particularly since all of these parameters affect each other and undergo time-dependent changes. This makes it also difficult to design effective strategies to promote tissue healing processes aimed at effectively inhibiting fibrotic processes which often impair organ function or lead to their failure. Guided by the different time-dependent phases of tissue remodeling seen in wound sites (Werner and Grose, 2003; Gurtner et al., 2008; Reinke and Sorg, 2012) and advances made in the fields of matrix and mechanobiology, the composition of the extracellular matrix, i.e. Fn-rich in early stages followed by increased collagen content,

* Corresponding author.
E-mail address: viola.vogel@hest.ethz.ch (V. Vogel).
[1] These authors contributed equally.

http://dx.doi.org/10.1016/j.matbio.2014.09.001

may direct fibroblasts through the different tissue maturation stages as Fn is mostly recognized by αVβ3 and α5β1 integrins, while fibroblasts bind to collagens among others via α2β1 integrins (Humphries et al., 2006). We thus asked how different ECM components (Fn and Col1) orchestrate differential MMP-expression and the time-dependent ECM remodeling by human foreskin fibroblasts (HFFs).

The focus on Fn is motivated by the fact that Fn is the major component of early ECM in matrix remodeling by fibroblasts (Clark, 1990; Mao and Schwarzbauer, 2005; Sottile et al., 2007; Hynes, 2009; Shaw and Martin, 2009). Fn consists of two almost identical Fn monomers, each approximately 220–250 kDa in molecular weight (Pankov and Yamada, 2002). It contains cell binding sites such as the RGD sequence that is recognized by surface receptor integrins (Pankov and Yamada, 2002; Mao and Schwarzbauer, 2005; Vogel, 2006; Hynes, 2009). Fn also contains various binding sites for ECM proteins such as Fn, type I and III collagen (Pankov and Yamada, 2002; Vogel, 2006). Fn therefore affects cell signaling by being recognized by the integrins α5β1 and αVβ3, while collagen associates with the integrins α1β1 and α2β1 (Humphries et al., 2006). Switching the attachment of cells from Fn to collagens exploiting different sets of integrins thus provides a means to alter cellular behavior (Kadler et al., 2008; Kennedy et al., 2008; Soucy and Romer, 2009; Seong et al., 2013).

We therefore hypothesize that the different tissue maturation stages, characterized by the time-variant changes in ECM composition, i.e. Fn-rich towards collagen-rich might tune fibroblast behavior and specifically their ECM repair and remodeling capacity. We looked into this question by observing HFFs in the presence or absence of uniaxial cyclic strain, since uniaxial cyclic strain is a known inducer of ECM remodeling, resulting in fibroblast reorientation (Dartsch et al., 1986; De et al., 2007; Jungbauer et al., 2008; Faust et al., 2011), cytoskeletal reorganization (Goldyn et al., 2009; Goldyn et al., 2010; Deibler et al., 2011), focal adhesion realignment (Carisey et al., 2013) and altered matrix composition (Gupta and Grande-Allen, 2006; Shelton and Rada, 2007; Kanazawa et al., 2009; Nguyen et al., 2009; Cha and Purslow, 2010; Foolen et al., 2012).

Finally, ECM integrity is affected by matrix metalloproteinases (MMPs) and tissue inhibitors of metalloproteinases (TIMPs) that play crucial roles during matrix remodeling. By regulating the degradation of ECM, MMPs and TIMPs have been considered pharmacological agents to promote healthy tissue remodeling (Lee and Murphy, 2004; Vihinen et al., 2005; Gill and Parks, 2008; Dufour and Overall, 2013). Several human MMPs were reported to interact with Fn, namely MMP-2 and 3, MMP-7, MMP-9-12, MMP-14, MMP-16, MMP-24-26 (Overall, 2002; Klein and Bischoff, 2011) and their activities can be inhibited by four different TIMPs (Visse and Nagase, 2003). MMP-2 and -9 (gelatinase-A and –B) are secreted as inactive soluble zymogens, degrade several ECM substrates such as gelatin, collagen and Fn (Toriseva and Kahari, 2009), and have been shown to be important for connective tissue remodeling (Romanic et al., 2002; Hayashidani et al., 2003; Zamilpa et al., 2010). In addition, MMP-14 and -15 are membrane-anchored endopeptidases activated once inserted into cell membranes (Itoh and Seiki, 2006; Sohail et al., 2008; Murphy and Nagase, 2011) that can digest ECM molecules that arein proximity to the cell membrane (Egeblad and Werb, 2002; Lee and Murphy, 2004; Chen and Parks, 2009). But to which extent matrix composition and/or stretch-regulated matrix conformations might affect differential expression and secretion of MMPs remains elusive. We therefore asked how exposing HFFs to exogenous collagen and/or Fn regulates their ECM remodeling capacity and whether this affects their secretion and activity of MMPs. Our approach was to explore how exposure of HFFs to Col1 and/or human plasma Fn (pFn) under cyclic stretch or rest, affected the assembly and remodeling of ECM. The cellular capacity to assemble, degrade and remodel matrix was assessed by confocal microscopy, MMP activity assays and gene expression analysis.

2. Results

2.1. HFFs assemble Fn matrix fibrils parallel to their long axis when subjected to uniaxial cyclic strain

HFFs were first grown on silicone sheets under static conditions for 16 hours in serum-free growth medium prior to the onset of cyclic stretching versus continued static conditions in the presence of 50 μg/mL plasma-Fn (pFn). Since fibroblasts are known to reorient upon the onset of uniaxial cyclic strain (Dartsch et al., 1986; Jungbauer et al., 2008), we first monitored how this impacts the process of de novo Fn fibrillogenesis by HFFs. On pFn coated substrates, unstretched cells were randomly oriented, whereas after 8 hours of uniaxial cyclic stretching (10% at 1Hz), the orientation of HFFs converged to angles close to 60°, i.e. close to the minimum strain direction (Fig. 1A), as previously observed by others (De et al., 2007; Jungbauer et al., 2008; Faust et al., 2011). In our case where we have applied 10% uniaxial cyclic strain to the unconfined Fn-coated polydimethylsiloxane (PDMS) substrate (Poisson's ratio = 0.5), the minimum strain direction was ~60° away from the stretching direction as a result of both stretching in the strain direction and compression perpendicular to the strain direction. In addition to a change in cellular orientation, cyclically stretched cells show a more spindle-like morphology (Aspect $Ratio_{Stretch} = 3.0$) compared to unstretched cells (Aspect $Ratio_{Rest} = 1.6$) (Fig. 1B). This strain-induced change in cellular morphology thus confirms previous reports (Deibler et al., 2011; Faust et al., 2011).

To monitor the directionality of assembled Fn fibers by HFFs under uniaxial cyclic stretching, trace amounts of fluorescently labeled pFn (50 μg/mL) were added to the culture media at the beginning of each experiment. Unstretched HFFs assembled Fn matrix in random orientations, whereas cyclically stretched HFFs assembled Fn fibrils mainly parallel to their long axis. The Fn fibril angle distribution also peaked around 60° away from the direction of applied strain (Fig. 1C). These results show that HFFs react to cyclic mechanical stretching by altering not only cell alignment, but also the orientation of the assembled Fn fibrils.

2.2. Cyclic stretching increased actin stress fiber formation and assembly of Fn matrix by HFFs

Since Fn fibrillogenesis is induced by translocation of α5β1 integrins along actin filaments (Katz et al., 2000; Pankov et al., 2000), the relation between Fn alignment and F-actin organization under cyclic strain was then quantified. After firm attachment onto pFn-coated PDMS substrates in Fn-depleted growth medium, HFFs were subjected to 4 hours of cyclic stretching (10% at 1Hz) and 50 μg/mL pFn was supplemented during stretching. Increased formation of actin stress fiber assembly was observed as visualized by antibody staining of F-actin (Fig. 2A). A strong linear correlation between the alignment of actin stress fibers and Fn fibers was detected in both unstretched (rest) samples ($R^2 = 0.8$) and stretched samples ($R^2 = 0.8$) (Fig. 2B). The strong correlation between F-actin and Fn suggests that the overall arrangement of Fn fibrils was dominated by the re-aligned actin network, not only for HFFs cultured at static conditions but also at uniaxial cyclic strain.

In addition to strain-induced alignment of new matrix fibers, cyclic stretching significantly increased the amount of Fn assembled from the growth medium by HFFs (8 hours of uniaxial cyclic stretching, Fig. 2C). Therefore, cyclic stretching promoted both, the formation of actin stress fibers and assembly of Fn matrix compared to the unstretched controls.

2.3. Cells predominantly assemble new Fn matrix aligned to their long axis, and remodel very little of the existing Fn matrix

Because of the strong correlation between the directionality of F-actin stress fibers and Fn fibrils, we asked how the HFFs change the

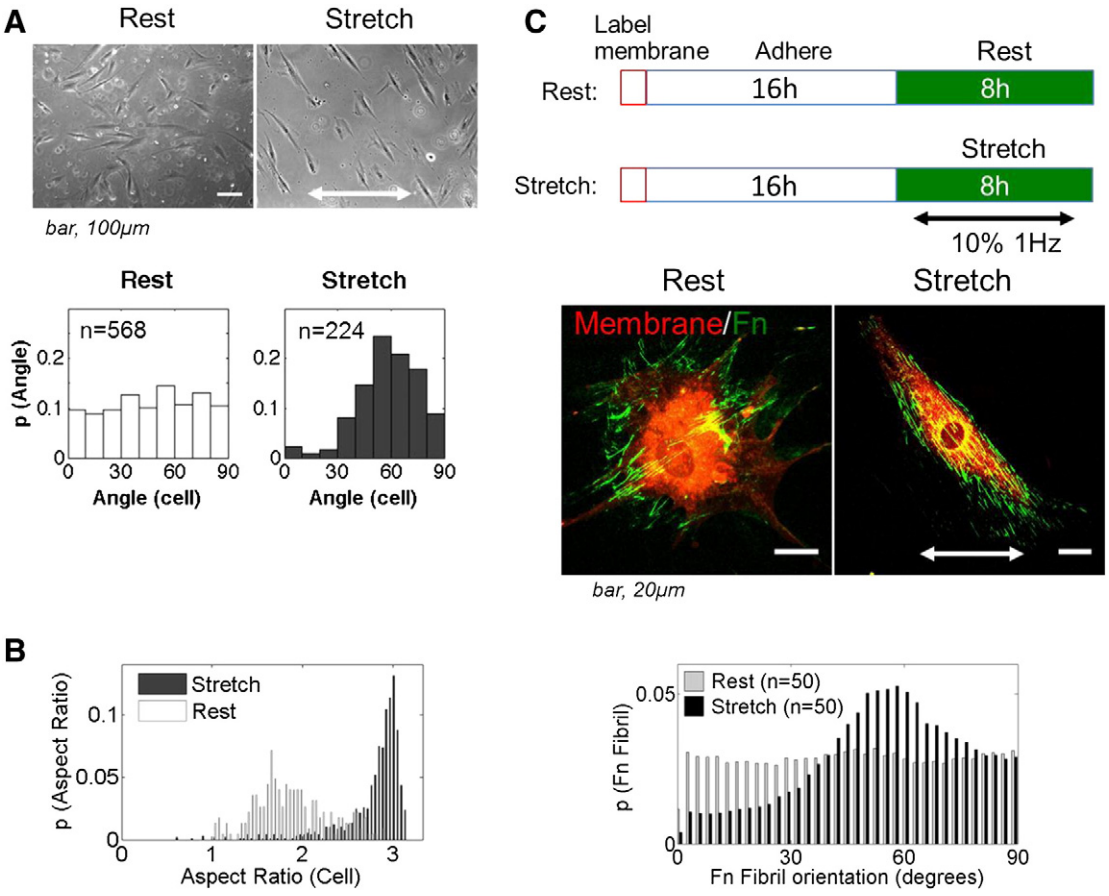

Fig. 1. HFFs assemble Fn matrix fibrils parallel to their long axis when subjected to uniaxial cyclic strain. HFFs were seeded in Fn coated PDMS chambers for 16 hours to ensure firm adhesion to the substrate. HFFs were then either exposed to cyclic stretching (stretch) or cultured at static conditions (rest). A) Under resting conditions, HFFs displayed a random orientation. Upon uniaxial cyclic stretching of 10% 1Hz for 8 hours, HFFs aligned to ~60°, which represents the minimal substrate deformation direction in this system since stretching over the 0 degree axis is accompanied by compression in the 90 degrees direction. The angle of cell orientation was obtained by fitting an ellipse to the cell. B) After 8 hours of uniaxial cyclic stretching (10%, 1 Hz), HFFs were more spindle-shaped as can be observed from the probability plot (Aspect $Ratio_{Stretch} = 3.0$) compared to unstretched cells (Aspect $Ratio_{Rest} = 1.6$). C) Top picture illustrates the experimental setup for monitoring Fn matrix assembly during cyclic stretching. Namely, pre-labeled Fn (green) was added to the growth media at 50 μg/mL. To visualize HFFs, cell membranes were labeled with a red membrane dye (DiI, Invitrogen, Switzerland) prior to seeding. Under resting conditions, HFFs assembled Fn matrix with a random orientation, as can be observed from the probability plot. Under uniaxial cyclic stretching, the HFFs also assembled Fn matrix preferentially along ~60°.

distribution of Fn fiber orientation. To distinguish between cyclic-strain-induced remodeling of old Fn matrix grown under static conditions and the assembly of new Fn matrix, a pulse-chase experiment was designed in which HFFs were cultured in the presence of green fluorescently labeled pFn under static conditions for 24 hours. Subsequently, cells were cyclically stretched for 8 hours (10% at 1Hz) in the presence of red fluorescently labeled pFn (Fig. 3A). Images were taken before (Fig. 3B) and after stretching (Fig. 3C and D). A quantitative analysis of the angular fiber distribution was performed to detect the orientation of old and new Fn fibers for all three cases. The analysis revealed that new fibers (red) compared to old (green) are predominantly aligned at angles around 60° (Fig. 3E–F, green versus red). As cells reorient in response to the onset of cyclic strain in the presence of a randomly aligned Fn-network, they hardly remodel the pre-existing matrix. Instead, they leave the old matrix and assemble new ECM with a different Fn fiber orientation.

To gain insight into why cells leave the pre-existing (old) matrix in response to the onset of cyclic strain, concentrations of secreted MMPs were measured in the growth media under stretching versus resting conditions. However, cyclic stretching did not result in major upregulation of soluble MMP activity as measured by a generic MMP-assay in the absence (Fn-) or presence (Fn+) of pFn (Fig. 3G). However, in the presence of pFn, a major increase of MMP secretion was observed (Fig. 3G). To get more insights into the type of MMPs responsible for these differences, the activity of secreted MMP-2 and MMP-9 (gelatinases) in the growth medium were analyzed by gelatin zymography. Most interestingly, stretching did not affect gelatinase activity, while the exposure to pFn increased MMP activity significantly (Fig. 3H). Therefore, MMP secretion and activity is not significantly upregulated by cyclic strain, but increases upon exposure to pFn.

2.4. Monomeric Type 1 collagen (Col1) added to the medium down-regulates MMP secretion by cyclically stretched HFFs

Since cells in vivo can only assemble collagen matrices in the presence of Fn (Kadler et al., 2008), and since the appearance of collagen in ECM typically changes several parameters at the same time, i.e. the ratio of ECM constituents, as well as the density/architecture/rigidity of the ECM, the ECM composition cannot be tuned easily without tuning all of these other parameters. To ask how the exposure to collagen affects MMP secretion by HFFs, we first allowed the cells to assemble a Fn matrix for 24 hours, and subsequently cultured the cells in medium that contained both pFn (50 μg/mL) and soluble monomeric rat-tail Col1 (5 μg/mL) for an additional 8 hours. Most interestingly, MMP secretion was down-regulated when cells were exposed to exogenously added Col1. HFFs secreted almost 3-fold more soluble MMPs when exposed to pFn (Fig. 4A), while Col1 in addition to pFn reduced the high pFn-induced MMP-levels (Fig. 4A, 2-fold increase compared to control).

To identify candidates of soluble MMPs that account for this observation, the activity of MMP-2 and MMP-9 (gelatinases) on the

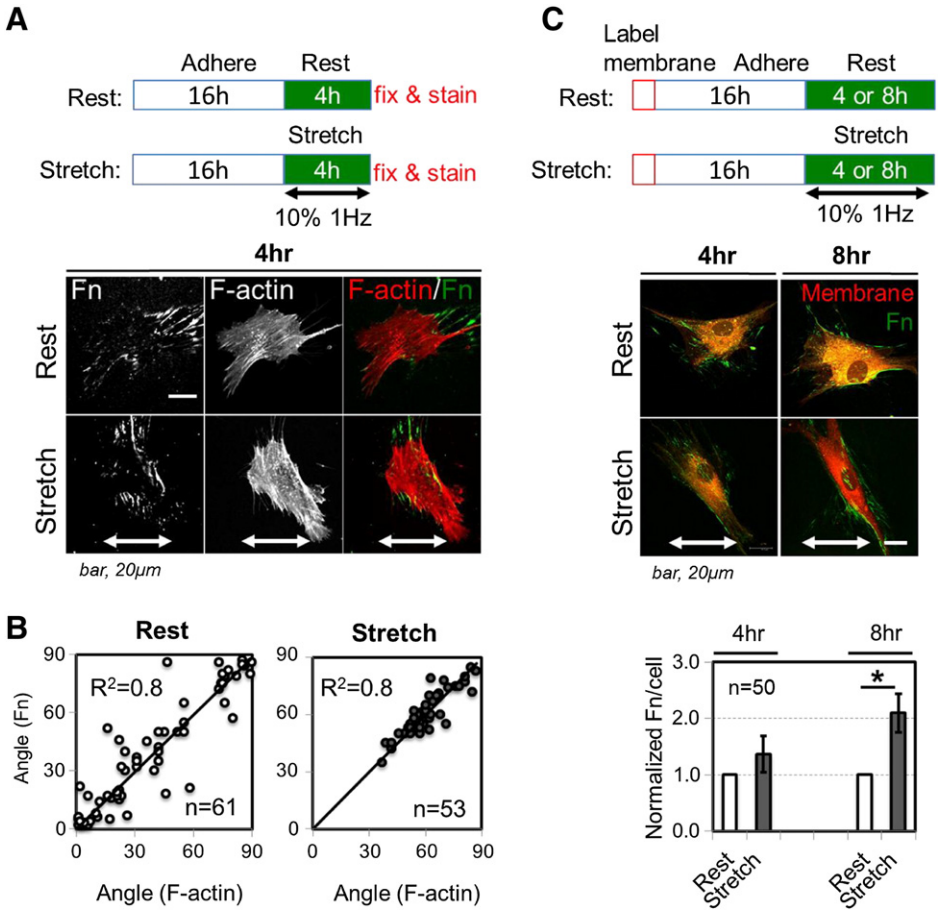

Fig. 2. Cyclic stretching increased actin stress fiber formation and assembly of Fn matrix by HFFs. A) HFFs were seeded onto Fn coated PDMS substrates (25 μg/mL Fn at 37 °C for 3 hours) for 16 hours. Then cells were stretched for 4 hours at 10% 1Hz, while being exposed to fluorescently labeled Fn (green). Phalloidin staining of F-actin reveals that uniaxial cyclic stretching promoted actin stress fiber formation in HFFs. B) With or without stretching, the orientation of actin stress fibers in HFFs and Fn fibrils deposited by HFFs were closely associated with each other ($R^2 = 0.8$ for rest, $R^2 = 0.8$ for stretch). C) HFFs, labeled in red, were cyclically stretched for 4 and 8 hours. Compared to HFFs cultured at rest, cyclically stretched HFFs deposited significantly more Fn matrix within 8 hours ($p < 0.05$, Student's t-test).

protein level was quantified by using gelatin zymography. The activity of MMP-9 was significantly increased by introducing Col1 and/or pFn to the culturing medium, whereas the level of MMP-2 was unaffected (Fig. 4B). However, MMP-9 activity in Fn-rich matrix was superior to that in the presence of monomeric Col1 (Fig. 4B). Taken together with the generic MMP and zymography measurements, HFFs have a higher capacity to degrade ECM than in the presence of monomeric Col1.

The generic MMP assay and gelatin zymography only measure the MMPs in supernatant and can therefore not assess the activity of membrane-anchored MT-MMPs. Therefore, gene expression levels of MT-MMPs and of TIMPs, as well as of the matrix proteins, i.e. Fn and of collagens, were assessed using Reverse Transcription-quantitative Polymerase Chain Reaction (RT-qPCR). In general, changes in expression levels were rather small upon uniaxial cyclic stretching. Nevertheless, addition of pFn slightly upregulated Fn and MMP-15 (transmembrane type I MMP) expression and slightly downregulated collagen expression (Fig. 4C) by HFFs. Exposure of HFFs to collagen in addition to plasma Fn appeared to abolish these effects (Fig. 4C).

2.5. Monomeric Col1 binds to Fn fibers and reduces HFF-induced Fn fiber tension

Since the addition of Col1 to cultures significantly reduced MMP secretion by HFFs (Fig. 4), we next asked how the presence of Col1 potentially impacts ECM signaling. Pre-labeled green pFn and red Col1 were added to static HFF cultures for 24 hours, after which co-localization was visualized by confocal microscopy. Increasing concentrations of monomeric Col1 (1, 5 and 10 μg/mL, Fig. 5A-C, D-F and G-I, respectively) increased the amount of Col1 co-localization with Fn fibers (Fig. 5C, F, I). Knowing that the mechanical strain of Fn fibers regulates the exposure of its binding sites (Zhong et al., 1998; Vogel, 2006; Little et al., 2009; Chabria et al., 2010; Lemmon et al., 2011), we also added trace amounts of FRET-labeled pFn as mechanical strain sensors (Baneyx et al., 2001; Smith et al., 2007; Little et al., 2008; Kubow et al., 2009) to probe the change in matrix conformation upon Col1 binding to the Fn ECM fibrils. FRET-labeled pFn was added to static HFF cultures for 24 hours in the absence or presence of Col1 (1, 5 or 10 μg/mL). Increasing concentrations of collagen increased the FRET intensity ratios, indicating that Fn was less stretched if the fibers where decorated with Col1 (Fig. 6A). Overlaid Fn FRET histograms and box plots showed that Col1-enriched ECM had higher Fn acceptor/donor intensity ratios with values above 0.70 compared to the control sample of 0.66 (Fig. 6B).

3. Discussion

Given the sparse information on how time-dependent alterations of early ECM during wound healing affect the activity of fibroblasts, we asked how matrix composition affects MMP production and matrix remodeling by HFFs that were either cultured under static conditions or subjected to uniaxial cyclic strain. HFFs responded to cyclic strain by re-aligning to the minimum strain direction, reinforcing their actin cytoskeleton, and assembling new Fn fibrils along their long axis (Figs. 1 and 2). Strikingly, MMP gene expression and activity were

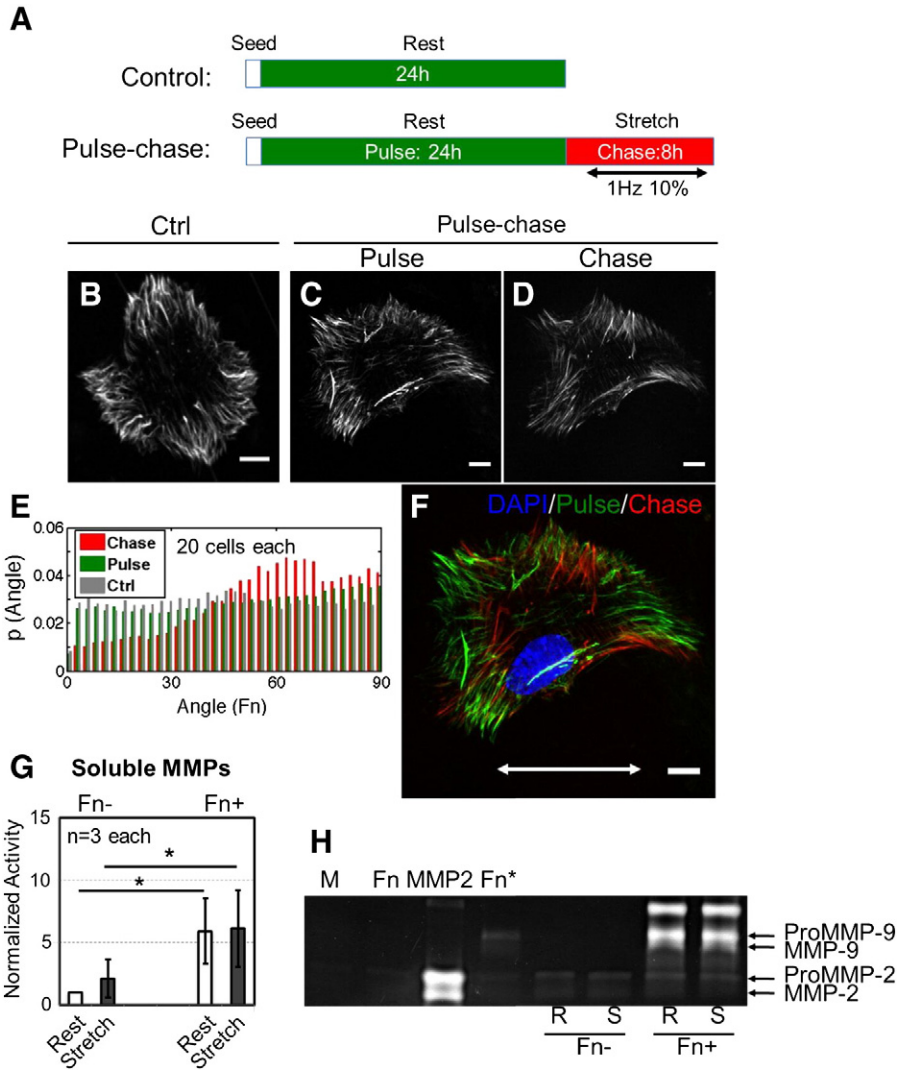

Fig. 3. Upon the onset of uniaxial cyclic stretch, HFFs predominantly assemble new Fn matrix aligned to their long axis, with minor remodeling of the old matrix. A) HFFs were plated onto Fn-coated PDMS substrates and were allowed to assemble matrix for 24 hours (50 μg/mL fluorescently labeled Fn (green) was added to the growth medium). Subsequently, HFFs were exposed to uniaxial cyclic strain at 10% 1 Hz for 8 hours, with fresh growth media containing fluorescently labeled Fn (red). B–F) Without stretching, ECM was assembled by HFFs with random Fn fiber orientation. After HFFs were stretched for 8 hours, the Fn fiber orientation showed slight preference towards angles around 60–90 degrees. HFFs preferred assembled Fn matrix along ~60° under uniaxial cyclic strain. Merged image of Fn matrix assembled before and during stretching showed that HFFs deposited new matrix preferentially along ~60° under uniaxial cyclic stretching. G) In the absence of exogenously added pFn, stretching slightly increased (non-significant) soluble MMP secretion. Exogenously added pFn (50 μg/mL) resulted in an increase in soluble MMP secretion, however equally for the resting and stretched cells. H) 8 hours of uniaxial cyclic stretching at 10% 1Hz did not affect the secretion of MMP-2 and -9 by HFFs. Contrary, adding exogenous Fn significantly increased the secretion of MMP-9.

highly dependent on cellular exposure to pFn in the medium, but far less to applied cyclic strain (Fig. 3). Exogenously added Col1 bound to existing Fn matrix fibrils (Fig. 5) and reduced the levels of secreted MMPs compared to Fn matrix (Fig. 4). Finally, collagen-decoration of Fn-fibers coincided with a more relaxed conformation of Fn (Fig. 6).

Whereas the formation and orientation of new Fn fibrils along the long axis of HFFs is in agreement with previous findings for Fn (Antia et al., 2008) or collagen assembly (Birk and Trelstad, 1984; Trelstad and Birk, 1985; Birk and Trelstad, 1986), our pulse-chase experiments showed that cells preferentially aligned new ECM fibrils and left existing matrix unaltered (Fig. 3). The HFFs thereby up-regulated Fn gene expression and assembly, which is in agreement with earlier studies in which an elevated Fn expression was found in response to mechanical loading in various types of fibroblasts (Howard et al., 1998; Fluck et al., 2003; Garvin et al., 2003; He et al., 2004). During this early stage, Col1 and Col3 expression was slightly decreased when cyclically stretched HFFs were exposed to exogenous Fn. At first glance, this seems to be in contrast to the general behavior that collagen levels are increased when cells are subjected to cyclic strain (Curwin et al., 1988; Parsons et al., 1999; Kim et al., 2002; Wang and Sanders, 2003; Yang et al., 2004). However, no Fn was supplemented via the medium in these previous studies. When exogenous Col1 was added, we observed that Col3 expression was slightly upregulated, while Col1 expression returned to control levels and Fn expression remained higher (Fig. 4C). Taken together, cyclically stretched HFFs appear to increase the gene expression of Fn during the build-up phase in which they assemble a provisional Fn matrix.

Compared to the observed tendency of upregulated MMP levels in response to cyclic strain, which is in agreement with previous findings (Prajapati et al., 2000), exposure of HFFs to exogenously added pFn in the medium had a far greater effect, specifically on MMP-9 activity (Fig. 4). It is particularly interesting to note that the membrane-bound MMP-15 is slightly up-regulated under conditions where we see that the HFFs, in response to the onset of cyclic strain, started to assemble a new ECM with a distinctly different fiber orientation.

Addition of Col1 to the medium, while keeping the high Fn concentrations, decreased MMP secretion by HFFs (Fig. 4). Increased MMP activity promoted local matrix degradation which might be

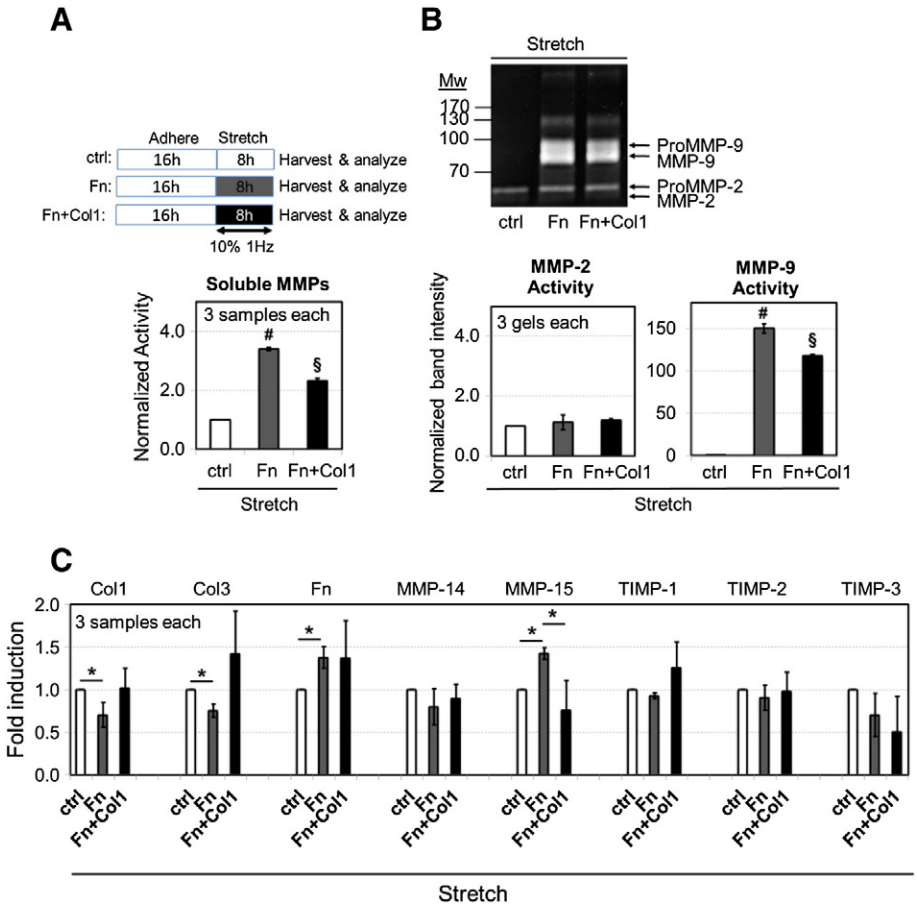

Fig. 4. Addition of monomeric collagen (Col1) in addition to Fn via growth medium, reduced MMP secretion by cyclically stretched HFFs. A) After 8 hours of uniaxial cyclic stretching at 10% 1Hz, HFFs secreted almost 3-fold more soluble MMPs when HFFs were exposed to 50 μg/mL Fn via the growth medium. The addition of Col1 and Fn via the medium resulted only in a 2-fold increase in soluble MMPs (# and § represent a significant difference with all other groups, $p < 0.05$, ANOVA). B) The increase in soluble MMP secretion due to Fn and Col1 addition was mainly contributed by MMP-9 not MMP-2. Again, MMP-9 secreted by HFFs as measured by gelatin zymography was lower for Col1 decorated Fn-matrix than Fn matrix alone (# and § represent a significant difference with all other groups, $p < 0.05$, ANOVA). C) At cyclic stretching conditions, gene expression of type I and III collagen was decreased by ~20% upon Fn matrix assembly, while Fn expression was increased by ~30%. The expression of MMP-15 was up-regulated by ~40%, whereas gene expression of HFFs in the presence of Col1 did not show any significant change compared to cells growing in normal growth media. * represent significant differences, $p < 0.05$, ANOVA.

particularly important in early stages of ECM repair in wound sites. But once tissue matures to include Col1, the cellular need for MMPs to remodel ECM might decrease. This hypothesis is supported by the specificity of MMP-15 for Fn, laminin and tenascin-C but for none of the collagens (d'Ortho et al., 1997). However, unlike cells in 3D collagen lattices (Haas et al., 1998; Ruangpanit et al., 2001; Wilkinson et al., 2012), we did not see significant up-regulation of MMP-14 expression with the increase of exogenously added Col1. We expect this discrepancy to originate from the different model systems used (including 2D vs 3D and associated differences in fiber diameter, rigidity and density), since in all our experiments, cells maintained their typical '2D' morphology.

How the presence of Col1 in early ECM in addition to Fn reduced MMP activity is unknown, but our data suggest a potentially synergetic mechanism. First, collagen monomers are known to bind to Fn-fibrils via Fn's gelatin binding site, and the appearance of collagens in ECM may allow cells to switch from the Fn binding integrins, particularly $\alpha5\beta1$, to collagen binding integrins, i.e. $\alpha2\beta1$ to anchor themselves in their ECM environments. This can alter associated downstream signaling pathways, thereby impacting cellular mechanosensing. For example, recent findings suggested that FAK activation on Fn-coated hydrogels was tension-dependent whereas activation on Col1 was tension-independent (Seong et al., 2013). Second, the incorporation of Col1 into Fn matrix also led to a more relaxed conformation of Fn in ECM, whereby it should be noted that FRET-Fn serves as a molecular strain and not a force probe. Relaxing the strain of fibrillar Fn in the presence of Col1 might tune how Fn fibrils act as mechano-tunable scaffolds, either by binding or by releasing growth factors and cytokines from its binding sites that are located on mechanoresponsive Fn repeats (Vogel, 2006; Hynes, 2009).

Could our reductionist approach perhaps suggest regulatory mechanisms of relevance to wound healing processes? While each wound healing model, from scratch assays to mouse knock-out models, puts the spotlight on one or another singular aspect, thereby neglecting many other co-regulatory stimuli, we looked into the question how HFFs are regulated by alterations of the dominant components of early ECM, i.e. Fn versus collagen-enriched ECM. Fn is the first provisional matrix actively assembled by fibroblasts at the site of injury (Clark, 1990; Shaw and Martin, 2009) and we find here that Fn ECM assembly is stimulated by the presence of high Fn concentrations in the medium. To reach tissue homeostasis though, fibroblasts ultimately need get tuned down. Our data suggest that the presence of Col1 in ECM might serve as such an extrinsic checkpoint signal as it decreased their MMP activity and the tension of Fn matrix fibrils.

4. Experimental procedures

4.1. Cell culture

Primary normal human dermal fibroblast, more commonly known as human foreskin fibroblasts (HFF; C-12300, Promocell, Germany) were maintained at 37 °C with 5% CO_2 in fibroblast growth medium

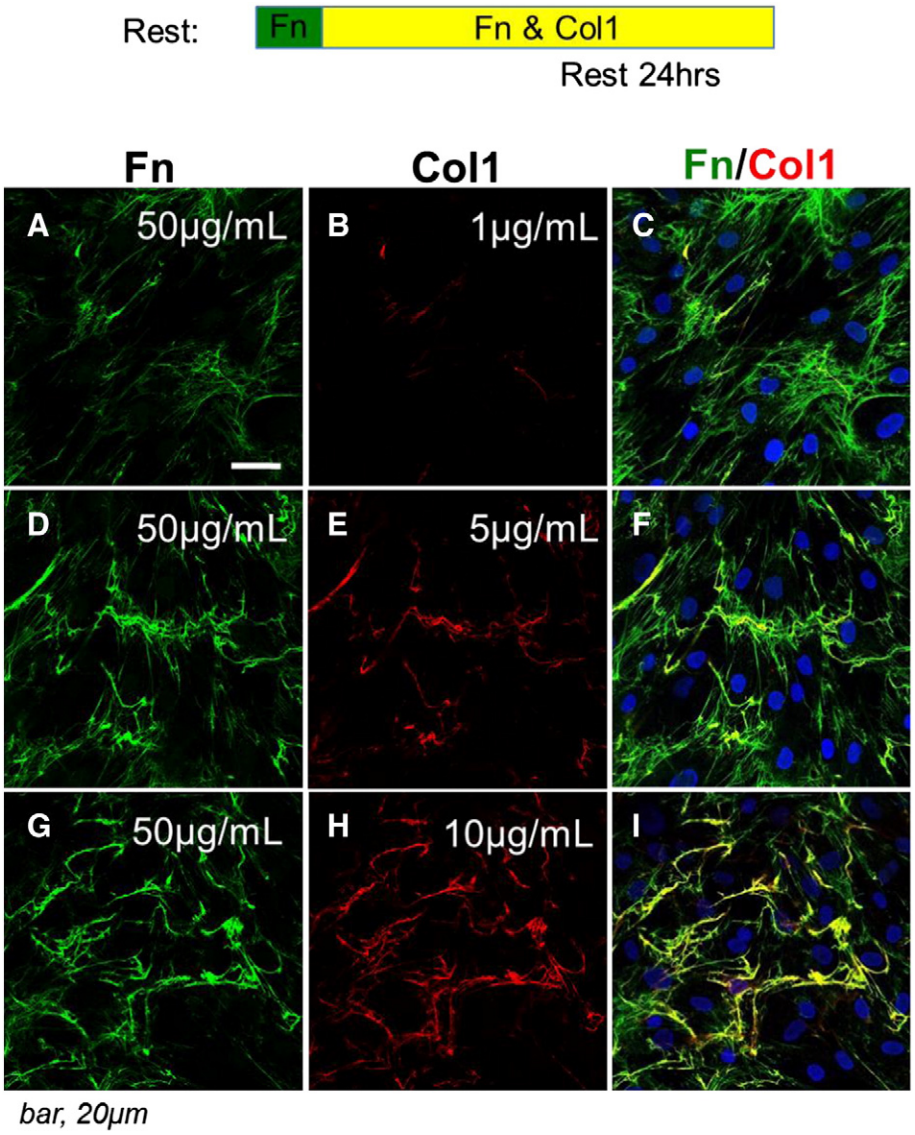

Fig. 5. Monomeric Col1 added to the medium binds to Fn ECM fibrils. HFFs were supplemented with 50 μg/mL pre-labeled Fn (green) for 30 minutes before adding 1, 5 or 10 μg/mL pre-labeled Type I collagen (Col1, depicted in red). Cells were allowed to assemble matrix for 24 hours before fixation. A-C) HFFs incorporated exogenous Fn (50 μg/mL) and monomeric Col1 (1 μg/mL) to assemble ECM. Cells assembled soluble Fn into fibrillar Fn matrix. Col1 co-localized with Fn fibrils. D-F, G-I) Col1 colocalization with Fn-fibrils increased with increasing Col1 concentrations in the medium (5 μg/mL and 10 μg/mL).

(C-23010, Promocell, Germany). This fibroblast growth medium does not contain serum but recombinant human fibroblast growth factor at 1 ng/ml and insulin at 5 μg/ml for a more consistent cell proliferation rate and better morphological maintenance. When HFFs reached 70–90% confluency, they were trypsinized by 0.05% trypsin-EDTA (25300–054, Invitrogen, Switzerland) and passaged at least once before being deployed in experiments. All experiments with HFF were carried out with cells below passage 10 to eliminate the appearance of myofibroblast phenotype at higher passage numbers.

4.2. Isolation of plasma fibronectin

Human plasma fibronectin (pFn) was isolated by gelatin affinity chromatography using a protocol adapted from a published method (Speziale et al., 2008). Briefly, frozen human plasma (Universitäts Spital Zurich, Switzerland) was thawed at 37 °C and protease inhibitor 2 mM PMSF (78830, Sigma-Aldrich, Switzerland) and 2 mM EDTA (ED-100G, Sigma-Aldrich, Switzerland) were added to prevent protein degradation. Plasma was centrifuged at 10,000 rpm for 20 min at 4 °C to eliminate debris and precipitation. Then, the plasma was passed through a column containing Sepharose 4B beads (4B200-500ML, Sigma-Aldrich, Switzerland) and subsequently a column containing 2 mM EDTA activated gelatin Sepharose 4B beads (45000170, Fisher Scientific, Switzerland). After binding, the gelatin column was washed with 500 mL 1 M NaCl (S9888, Sigma-Aldrich, Switzerland), 500 mL Phosphate buffer saline (PBS) (P4417, Sigma-Aldrich, Switzerland) pH7.4 containing 2 mM PMSF and 2 mM EDTA, and 500 mL 1 M urea. Gelatinases were eluded by washing the column with 500 mL 3% DMSO (Pal et al., 2010), and pFn was eluted with 3 M urea and stored at −80 °C. Before adding pFn to cell culture, pFn was dialyzed in PBS pH7.4 by using the 10 kDa molecular weight cut-off dialysis cassette (66380, Thermo Scientific, U.S.A.) to eliminate the urea and small Fn fragments.

4.3. Labeling of plasma fibronectin and collagen

Labeling of pFn was done following previous procedures (Smith et al., 2007). Briefly, for pFn (single or FRET) labeling, green fluorescent dye Alexa fluor 488 (A-20100, Invitrogen, Switzerland) and far-red fluorescent dye Alexa fluor 633 (A20105, Invitrogen, Switzerland)

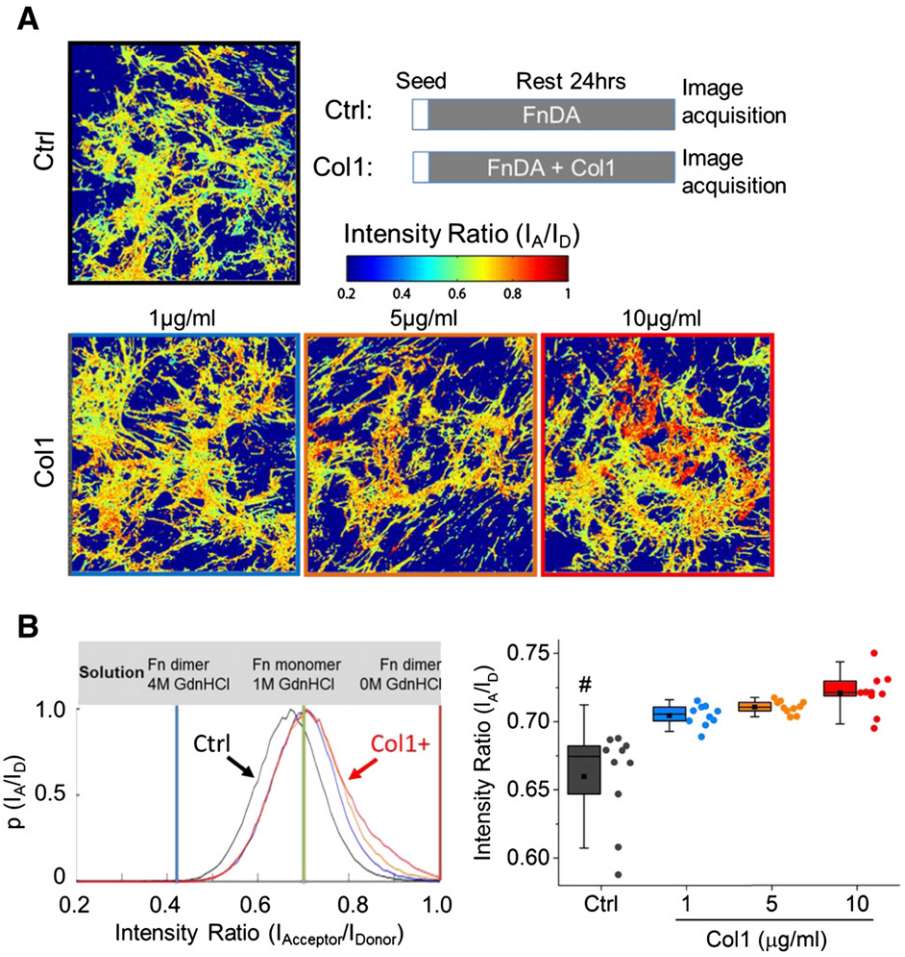

Fig. 6. Addition of monomeric Col1 decreased HFF-induced Fn fiber stretching. HFFs were seeded in Fn-depleted growth medium for 30 min before adding FRET-labeled Fn (Fn-DA). To prevent intermolecular FRET, 5 μg/mL Fn-DA was mixed with 45 μg/mL unlabeled Fn. For control samples, HFFs were supplemented with 5 μg/mL Fn-DA and 45 μg/mL unlabeled Fn. For Col1 samples, an additional 1, 5 or 10 μg/mL Col1 was added. Live images of matrix conformation were acquired after 24 hours of matrix assembly. A) Representative image of HFFs incorporating Fn-DA into Fn-rich and Col1-decorated matrix. Heat map images of the intensity ratio of acceptor and donor indicates the degree of unfolding, showing that Fn matrix fibrils were less unfolded once monomeric Col1 was added to the growth media compared to the control sample. B) Overlaid pixel-by-pixel FRET histograms of the images shown in (A) and box plots show that Col1-decorated matrices peaked at higher acceptor/donor intensity ratios (i.e. 0.7 versus 0.66). Denaturing of FRET-labeled Fn in solution by GdnHCl (as indicated in the gray bar), or the stretching of Fn ECM fibrils by cells, increases the overall distances of our multiple donors and acceptors per Fn-dimer (see method section for labeling protocol), thus reducing FRET. Box plots contain individual data points (filled circles) which represent the average FRET intensity ratio per measured image, or I_A/I_D. Boxplots further consist of the mean of the complete dataset (square), median (line), 25 and 75% (box), standard deviations (whiskers). # represents a significant difference with all other groups ($p < 0.05$, ANOVA).

were bound using NHS chemistry. Briefly, pFn was first dialyzed in 2 L labeling buffer consisting 0.1 M sodium bicarbonate (S5761, Sigma-Aldrich, Switzerland) PBS pH8.5 for 1.5 hours and then further dialyzed in 1 L fresh labeling buffer for 1.5 hours, both at room temperature. After dialysis, Fn concentration was determined by measuring the absorbance at 280 nm (NanoDrop 2000, Thermo Scientific, U.S.A.). Then 20 fold molar excess of Alexa fluor 488 or 633 carboxylic acid, succinimidyl ester was added. Because pFn is sensitive to mechanical stress, mixing was done by gently inverting the tubes. The mixture was then incubated in the dark for 1 hour at room temperature. Finally, labeled pFn was separated from free dyes by passing through the PD-10 desalting column (17-0851-01, GE Healthcare, U.K.). Labeled pFn was stored at −80 °C.

For the FRET studies, pFn was dual labeled with donors and acceptors. Given the large size of Fn exceeding 100 nm, multiple donors and acceptors per dimer were used to increase the range of conformational changes that can be detected by FRET even though this prevents us from calculating distances from FRET efficiencies. Alexa Fluor 488 fluorophores (FRET donors) were randomly bound to amines via succinimidyl ester chemistry and Alexa Fluor 546 fluorophores (FRET acceptors) were specifically targeted to the cryptic cysteins on the Fn type III modules $FnIII_7$ and $FnIII_{15}$ via maleimide chemistry (Molecular Probes), as previously described (Baneyx et al., 2002; Smith et al., 2007; Little et al., 2008; Kubow et al., 2009; Legant et al., 2012). The donor/acceptor labeling ratio of this Fn-DA was determined by measuring the absorbance of at 280, 498 and 556 nm. We obtained on average, 7 donors and 3.8 acceptors per pFn dimer. This Fn-DA was stored in PBS at −80 °C and used immediately upon thawing on ice. For consistent FRET results, FRET-labeled pFn from the same batch was used for all experiments shown here, and we quantified the intensity ratios of the acceptor versus donor emissions for FRET-labeled pFn either in physiological buffer, and upon denaturation with GndHCl, or after incorporation by cells into their ECM.

Collagen I (Col1) monomer from rat tail (BD Biosciences, Switzerland) was kept in 0.5 M acetic acid at 4 °C till usage. The monomer solution was dialyzed in borate buffer saline (pH8.2) overnight for pH adjustment. Concentration of dialyzed Col1 was determined by using BCA protein assay (Thermo Scientific, Switzerland). Then, 20-fold molar excess Alexa Fluoro 633 (Invitrogen, Switzerland) was added to the dialyzed Col1 and incubated at room temperature in the

dark for 1 hour. To separate labeled Col1 from free dyes in solution, the mixture was dialyzed in 0.1 N acerbic acid for 4 days at 4 °C in the dark.

4.4. Preparation of the PDMS chambers for stretch assays

Polydimethylsiloxane (PDMS) chambers were made by mixing the elastomer and curing agent at 10:1 (w/w) ratio (SYLGARD® 184 silicone elastomer kit, Dow Corning, U.S.A.). The mixture was degassed for 1 hour, and injected into custom made molds. The PDMS was baked at 80 °C for 4 hours to ensure complete crosslinking. After baking, the chambers were rigorously rinsed with 70% ethanol and Nanopure water (D11031, Thermo Scientific, U.S.A.) and sterilized by autoclaving at 121 °C for 20 minutes. Because PDMS surfaces are hydrophobic, 25 μg/ml pFn was used to coat the chambers to enable cell adhesion. Chambers were coated at 37 °C for 3 hours and washed gently with PBS to eliminate loosely bound pFn. HFFs were seeded at 5,000 cells/cm^2 for immunofluorescence experiments and 10,000 cells/cm^2 for MMP experiments in DMEM supplemented with 1% (v/v) Fn-depleted FBS and 1% (v/v) penicillin streptomycin (P/S) (15140–122, Invitrogen, Switzerland). HFFs were allowed to adhere and spread overnight. To visualize the deposition of Fn matrix before and during mechanical stretching, 50 μg/ml labeled pFn was added to the medium. HFFs were cyclically stretched at 1Hz to a maximum strain of 10% for 8 hours (37 °C, 5% CO_2) using the stretcher STREX ST-140 (B- Bridge International, U.S.A) which applies sinusoidal uniaxial strain to the PDMS chambers. The STREX ST-140 was purchased with a validated set of sinusoidal strain profiles. Two chamber sizes were used, the 4 cm^2 (2 cm × 2 cm) chambers for microscopy imaging, and the 10 cm^2 (3.33 cm × 3.33 cm) for biochemical assays (containing enough cells to perform these assay). In addition, STREX holds multiple chambers (5 × 10 cm^2 chambers, 6 × 4 cm^2 chambers), allowing parallel conditions within one set of experiments.

4.5. Microscopy and quantitative image analysis

Fluorescent samples were imaged with a Leica SP5 confocal microscopy system using a 20×/0.7 N.A. air objective or 63×/1.4 N.A. oil objective. Detectors accepted wavelengths of 498-530 nm, 570-630 nm and 643-800 nm for the different probes. For Z-stack, samples were imaged at every 300 nm from top to bottom. Maximal projection imaging was employed to visualize overall staining using ImageJ (National Institute of Health).

Quantitative image analysis was performed using ImageJ and custom-written software in MATLAB (MathWorks) or Mathematica (Wolfram Research). Cell orientation and elongation was analyzed by thresholding DiI fluorescent images, followed by conversion to a binary mask, and approximation of the cell outline by fitting an ellipse. The aspect ratio was defined as the ratio between major to minor axis. Cell orientation was defined as the orientation of the major axis relative to the external direction of uniaxial strain. For analyzing the orientation of actin or Fn fibers, fluorescent phalloidin/Fn grayscale images were pre-processed by normalizing their values between 0 and 1 and padding them into all directions by 2 rows/columns. Filter kernels were constructed based on normalized 5×5 Sobel kernels in x direction (Sx) and y direction (Sy). Three filtered images were created by convolution of the rescaled image with the 2nd derivative kernels Sx*Sx, Sy*Sy, and Sx*Sy. Local orientation was computed for each pixel in the image by taking the arcus tangens of the following combination:

$$\alpha = 1/2 \cdot \arctan(-2I[Sx * Sy]/(I[Sx * Sx] - I[Sy * Sy]))$$

resulting in angles between 0° and 180°. For restricting the orientation analysis to fibers, masks were generated by applying a 3x3 Laplace filter to the grayscale fiber images, automatically thresholding the filtered images by the method of Otsu, and binarizing the result. For non-zero pixels in the masks, the angles in the corresponding orientation image were pooled. For Figs. 1B and 3F, pixel angles larger than 90° were folded back onto the range from 0° to 90° by setting the angle to 180° minus α, pixel values from several cells were pooled and depicted as histograms. For Fig. 2B, all angles from pixels in fibers in/around a single cell were pooled into a histogram that then was fitted by a normal distribution to determine the principal orientation. Orientations were projected onto the range from 0° to 90°, and pairs of average actin/Fn angles for the individual cells were depicted as points in the scatter plots.

All Fluorescent Resonance Energy Transfer (FRET) images were acquired from living cell samples. Images were acquired with an Olympus FV1000 confocal microscopy using a 40×/1.25 N.A. water immersion objective. Acceptor and donor intensities were quantified using 12-nm bandwidths across the donor (514–526 nm) and acceptor (566–578 nm) emission peaks, as previously described (Smith et al., 2007). Multiple regions of interest (ROIs) were acquired from each sample. In each region, FRET images were acquired throughout the entire Z-stack with a slice-to-slice distance of 1 μm. Images were processed with self-written Matlab codes, as previously described (Smith et al., 2007).

4.6. Generic MMP activity measurements and zymography

The activity of soluble MMPs was measured by the generic MMP assay (SensoLyte, ANASPEC, U.S.A.). Gelatin and casein zymography was performed according to the protocol published by Hu and Beeton (Hu and Beeton, 2010). Briefly, culture medium of each sample was obtained, centrifuged at 2000 rpm, 4 °C for 10 minutes to eliminate debris. Supernatant was then collected for gelatin or casein zymography. Samples were mixed with Tris-Glycine SDS sample buffer (LC2676, Invitrogen, Switzerland) on ice and loaded to 10% Tris-Glycine gel with 0.1% gelatin (EC6175BOX, Invitrogen, Switzerland). Gels were run in the Tris-Glycine SDS running buffer (LC2675, Invitrogen, Switzerland) using XCell Surelock Mini-Cell system (EI0001, Invitrogen, Switzerland) at constant voltage of 125 V for 90 minutes. After gel electrophoresis, gels were exposed to 100 mL renaturing buffer (LC2670, Invitrogen, Switzerland) with gentle agitation at room temperature for 30 minutes, followed by overnight incubation at 37 °C in the development buffer. Gels were carefully rinsed with deionized water three times and scanned to record the positions of molecular standard bands before SimplyBlue staining (LC6060, Invitrogen, Switzerland). Intensity of the bands was analyzed using ImageJ.

4.7. Reverse transcription-quantitative polymerase chain reaction (RT-qPCR)

After mechanical stretching, cell pellets were immediately washed, collected and stored at −80 °C. Cells were lysed, shredded by QIAshredder (79656, Qiagen, Switzerland) and RNA was isolated by the RNeasy procedure (74104, Qiagen, Switzerland). RNA quality was assessed by measuring the absorbance of each sample at wavelength of 230 nm, 260 nm and 280 nm, and only samples with 260/280 and 260/230 values between 1.9-2.1 were used for cDNA synthesis. RNA was reverse-transcribed with iScript™ Advanced cDNA Synthesis Kit for RT-qPCR (170–8842, Bio-rad, U.S.A.). cDNA, primers and SsoAdvanced™ SYBR® Green Supermix (172–5261, Bio-rad, U.S.A.) were mixed and genes were amplified on CFX Connect™ Real-Time System (185–5200, Bio-rad, U.S.A.). Primer sequences used for the experiments are listed in the table below (table 1), and synthesized by Microsynth (Microsynth, Switzerland).

Author contributions

Y.Z. and Z.L. designed, performed experiments and analyzed the data. Y.Z., J.F., I.S., M.W. and V.V. wrote the manuscript. I.S. provided tools for fiber orientation analysis. A.S. measured soluble MMP

Table 1
Used primer sequences.

	Accession No.	Sequence (5'-3')
GAPDH Forward	J02642.1	GCGGGGCTCTCCAGAACATCAT
GAPDH Reverse		GACGCCTGCTTCACCACCTTCTT
COL1A1 Forward	NM_000088.3	CATGACCGAGACGTGTGGAAACC
COL1A1 Reverse		CATGACCGAGACGTGTGGAAACC
COL3A1, F	NM_000090.3	GGATCAGGCCAGTGGAAATGTAAAGA
COL3A1, R		CTTGCGTGTTCGATATTCAAAGACTGTT
FN Forward	NM_002026.2	TCTCCTGCCTGGTACAGAATATGTAGTGAG
FN Reverse		GGTCGCAGCAACAACTTCCAGGT
MMP14 Forward	NM_004995.2	CCCAGCCCACCCATTGAAGTCT
MMP14 Reverse		CCCGACATCCCTCTCCTCTTGC
MMP15 Forward	NM_002428.2	CGACTGGGGCAGGGTGTTTAGA
MMP15 Reverse		GACAGTCTCCAACTGGGCAAAGAGAG
TIMP1 Forward	NM_003254.2	TGGAAAACTGCAGGATGGACTCTTG
TIMP1 Reverse		CAGGGGATGGATAAACAGGGAAACA
TIMP2 Forward	NM_003255.4	GGCAAGATGCACATCACCCTCTGT
TIMP2 Reverse		GTTCTTCTCTGTGACCCAGTCCATCC
TIMP3 Forward	NM_000362.4	CTAGACTGGTGAATTGGGGGAAATAGAA
TIMP3 Reverse		GCAGGACTTGGGGTGAAGTAAATGG
MMP2, Forward	NM_004530.4	CCTCCCGGTGCCCAAGAATAGA
MMP2, Reverse		GGCTCTGAGGGTTGGTGGGATT

concentrations for HFFs in Fn matrix. All authors have seen and edited the manuscript.

Competing financial interests

The authors declare no competing financial interests.

Acknowledgements

We gratefully acknowledge Dr. Bojun Li for his help with isolating human plasma fibronectin, and Cameron Moshfegh for helping with the designing of primers and his expertise on RT-qPCR. This project was funded by an ERC Advanced Grant No. 233157 (VV), as well as the EU grant NanoCard No. 229294, the SwissTransMed grant 33/2013 LifeMatrix. Jasper Foolen has received funding from the European Union Seventh Framework Programme (FP7/2007-2013) under grant agreement n°. PIEF-GA-2013-628585.

References

Aarabi, S., Bhatt, K.A., Shi, Y., Paterno, J., Chang, E.I., Loh, S.A., Holmes, J.W., Longaker, M.T., Yee, H., Gurtner, G.C., 2007. Mechanical load initiates hypertrophic scar formation through decreased cellular apoptosis. FASEB J. 21, 3250–3261.

Antia, M., Baneyx, G., Kubow, K.E., Vogel, V., 2008. Fibronectin in aging extracellular matrix fibrils is progressively unfolded by cells and elicits an enhanced rigidity response. Faraday Discuss. 139, 229–249.

Baneyx, G., Baugh, L., Vogel, V., 2001. Coexisting conformations of fibronectin in cell culture imaged using fluorescence resonance energy transfer. Proc. Natl. Acad. Sci. U. S. A. 98, 14464–14468.

Baneyx, G., Baugh, L., Vogel, V., 2002. Fibronectin extension and unfolding within cell matrix fibrils controlled by cytoskeletal tension. Proc. Natl. Acad. Sci. U. S. A. 99, 5139–5143.

Birk, D.E., Trelstad, R.L., 1984. Extracellular compartments in matrix morphogenesis: collagen fibril, bundle, and lamellar formation by corneal fibroblasts. J. Cell Biol. 99, 2024–2033.

Birk, D.E., Trelstad, R.L., 1986. Extracellular compartments in tendon morphogenesis: collagen fibril, bundle, and macroaggregate formation. J. Cell Biol. 103, 231–240.

Bryers, J.D., Giachelli, C.M., Ratner, B.D., 2012. Engineering biomaterials to integrate and heal: the biocompatibility paradigm shifts. Biotechnol. Bioeng. 109, 1898–1911.

Carisey, A., Tsang, R., Greiner, A.M., Nijenhuis, N., Heath, N., Nazgiewicz, A., Kemkemer, R., Derby, B., Spatz, J., Ballestrem, C., 2013. Vinculin regulates the recruitment and release of core focal adhesion proteins in a force-dependent manner. Curr. Biol. 23, 271–281.

Cha, M.C., Purslow, P.P., 2010. The activities of MMP-9 and total gelatinase respond differently to substrate coating and cyclic mechanical stretching in fibroblasts and myoblasts. Cell Biol. Int. 34, 587–591.

Chabria, M., Hertig, S., Smith, M.L., Vogel, V., 2010. Stretching fibronectin fibres disrupts binding of bacterial adhesins by physically destroying an epitope. Nat. Commun. 1, 135.

Chen, P., Parks, W.C., 2009. Role of matrix metalloproteinases in epithelial migration. J. Cell. Biochem. 108, 1233–1243.

Chiquet, M., Gelman, L., Lutz, R., Maier, S., 2009. From mechanotransduction to extracellular matrix gene expression in fibroblasts. Biochim. Biophys. Acta 1793, 911–920.

Clark, R.A., 1990. Fibronectin matrix deposition and fibronectin receptor expression in healing and normal skin. J. Investig. Dermatol. 94, 128S–134S.

Cox, T.R., Erler, J.T., 2011. Remodeling and homeostasis of the extracellular matrix: implications for fibrotic diseases and cancer. Dis. Models Mech. 4, 165–178.

Curwin, S.L., Vailas, A.C., Wood, J., 1988. Immature tendon adaptation to strenuous exercise. J. Appl. Physiol. 65, 2297–2301.

da Rocha-Azevedo, B., Ho, C.H., Grinnell, F., 2013. Fibroblast cluster formation on 3D collagen matrices requires cell contraction dependent fibronectin matrix organization. Exp. Cell Res. 319, 546–555.

Dartsch, P.C., Hammerle, H., Betz, E., 1986. Orientation of cultured arterial smooth muscle cells growing on cyclically stretched substrates. Acta Anat. (Basel) 125, 108–113.

De, R., Zemel, A., Safran, S.A., 2007. Dynamics of cell orientation. Nat. Phys. 3, 655–659.

Deibler, M., Spatz, J.P., Kemkemer, R., 2011. Actin fusion proteins alter the dynamics of mechanically induced cytoskeleton rearrangement. PLoS One 6, e22941.

Dideriksen, K., Sindby, A.K., Krogsgaard, M., Schjerling, P., Holm, L., Langberg, H., 2013. Effect of acute exercise on patella tendon protein synthesis and gene expression. Springerplus 2, 109.

d'Ortho, M.P., Will, H., Atkinson, S., Butler, G., Messent, A., Gavrilovic, J., Smith, B., Timpl, R., Zardi, L., Murphy, G., 1997. Membrane-type matrix metalloproteinases 1 and 2 exhibit broad-spectrum proteolytic capacities comparable to many matrix metalloproteinases. Eur. J. Biochem. 250, 751–757.

Dufour, A., Overall, C.M., 2013. Missing the target: matrix metalloproteinase antitargets in inflammation and cancer. Trends Pharmacol. Sci. 34, 233–242.

Egeblad, M., Werb, Z., 2002. New functions for the matrix metalloproteinases in cancer progression. Nat. Rev. Cancer 2, 161–174.

Faust, U., Hampe, N., Rubner, W., Kirchgessner, N., Safran, S., Hoffmann, B., Merkel, R., 2011. Cyclic stress at mHz frequencies aligns fibroblasts in direction of zero strain. PLoS One 6, e28963.

Fluck, M., Giraud, M.N., Tunc, V., Chiquet, M., 2003. Tensile stress-dependent collagen XII and fibronectin production by fibroblasts requires separate pathways. Biochim. Biophys. Acta 1593, 239–248.

Foolen, J., Deshpande, V.S., Kanters, F.M., Baaijens, F.P., 2012. The influence of matrix integrity on stress-fiber remodeling in 3D. Biomaterials 33, 7508–7518.

Gabbiani, G., 2003. The myofibroblast in wound healing and fibrocontractive diseases. J. Pathol. 200, 500–503.

Garvin, J., Qi, J., Maloney, M., Banes, A.J., 2003. Novel system for engineering bioartificial tendons and application of mechanical load. Tissue Eng. 9, 967–979.

Geiger, B., Spatz, J.P., Bershadsky, A.D., 2009. Environmental sensing through focal adhesions. Nat. Rev. Mol. Cell Biol. 10, 21–33.

Gill, S.E., Parks, W.C., 2008. Metalloproteinases and their inhibitors: regulators of wound healing. Int. J. Biochem. Cell Biol. 40, 1334–1347.

Goldyn, A.M., Rioja, B.A., Spatz, J.P., Ballestrem, C., Kemkemer, R., 2009. Force-induced cell polarisation is linked to RhoA-driven microtubule-independent focal-adhesion sliding. J. Cell Sci. 122, 3644–3651.

Goldyn, A.M., Kaiser, P., Spatz, J.P., Ballestrem, C., Kemkemer, R., 2010. The kinetics of force-induced cell reorganization depend on microtubules and actin. Cytoskeleton (Hoboken) 67, 241–250.

Gupta, V., Grande-Allen, K.J., 2006. Effects of static and cyclic loading in regulating extracellular matrix synthesis by cardiovascular cells. Cardiovasc. Res. 72, 375–383.

Gurtner, G.C., Werner, S., Barrandon, Y., Longaker, M.T., 2008. Wound repair and regeneration. Nature 453, 314–321.

Haas, T.L., Davis, S.J., Madri, J.A., 1998. Three-dimensional type I collagen lattices induce coordinate expression of matrix metalloproteinases MT1-MMP and MMP-2 in microvascular endothelial cells. J. Biol. Chem. 273, 3604–3610.

Hayashidani, S., Tsutsui, H., Ikeuchi, M., Shiomi, T., Matsusaka, H., Kubota, T., Imanaka-Yoshida, K., Itoh, T., Takeshita, A., 2003. Targeted deletion of MMP-2 attenuates early LV rupture and late remodeling after experimental myocardial infarction. Am. J. Physiol. Heart Circ. Physiol. 285, H1229–H1235.

He, Y., Macarak, E.J., Korostoff, J.M., Howard, P.S., 2004. Compression and tension: differential effects on matrix accumulation by periodontal ligament fibroblasts in vitro. Connect. Tissue Res. 45, 28–39.

Howard, P.S., Kucich, U., Taliwal, R., Korostoff, J.M., 1998. Mechanical forces alter extracellular matrix synthesis by human periodontal ligament fibroblasts. J. Periodontal Res. 33, 500–508.

Hu, X., Beeton, C., 2010. Detection of functional matrix metalloproteinases by zymography. J. Vis. Exp. 8 (pii 2445).

Humphries, J.D., Byron, A., Humphries, M.J., 2006. Integrin ligands at a glance. J. Cell Sci. 119, 3901–3903.

Hynes, R.O., 2009. The extracellular matrix: not just pretty fibrils. Science 326, 1216–1219.

Itoh, Y., Seiki, M., 2006. MT1-MMP: a potent modifier of pericellular microenvironment. J. Cell. Physiol. 206, 1–8.

Jungbauer, S., Gao, H., Spatz, J.P., Kemkemer, R., 2008. Two characteristic regimes in frequency-dependent dynamic reorientation of fibroblasts on cyclically stretched substrates. Biophys. J. 95, 3470–3478.

Kadler, K.E., Hill, A., Canty-Laird, E.G., 2008. Collagen fibrillogenesis: fibronectin, integrins, and minor collagens as organizers and nucleators. Curr. Opin. Cell Biol. 20, 495–501.

Kanazawa, Y., Nomura, J., Yoshimoto, S., Suzuki, T., Kita, K., Suzuki, N., Ichinose, M., 2009. Cyclical cell stretching of skin-derived fibroblasts downregulates connective tissue growth factor (CTGF) production. Connect. Tissue Res. 50, 323–329.

Katz, B.Z., Zamir, E., Bershadsky, A., Kam, Z., Yamada, K.M., Geiger, B., 2000. Physical state of the extracellular matrix regulates the structure and molecular composition of cell-matrix adhesions. Mol. Biol. Cell 11, 1047–1060.

Kennedy, L., Shi-Wen, X., Carter, D.E., Abraham, D.J., Leask, A., 2008. Fibroblast adhesion results in the induction of a matrix remodeling gene expression program. Matrix Biol. 27, 274–281.
Kim, S.G., Akaike, T., Sasagaw, T., Atomi, Y., Kurosawa, H., 2002. Gene expression of type I and type III collagen by mechanical stretch in anterior cruciate ligament cells. Cell Struct. Funct. 27, 139–144.
Kippenberger, S., Bernd, A., Loitsch, S., Guschel, M., Muller, J., Bereiter-Hahn, J., Kaufmann, R., 2000. Signaling of mechanical stretch in human keratinocytes via MAP kinases. J. Investig. Dermatol. 114, 408–412.
Klein, T., Bischoff, R., 2011. Active metalloproteases of the A Disintegrin and Metalloprotease (ADAM) family: biological function and structure. J. Proteome Res. 10, 17–33.
Kubow, K.E., Klotzsch, E., Smith, M.L., Gourdon, D., Little, W.C., Vogel, V., 2009. Crosslinking of cell-derived 3D scaffolds up-regulates the stretching and unfolding of new extracellular matrix assembled by reseeded cells. Integr. Biol. (Camb.) 1, 635–648.
Lee, M.H., Murphy, G., 2004. Matrix metalloproteinases at a glance. J. Cell Sci. 117, 4015–4016.
Legant, W.R., Chen, C.S., Vogel, V., 2012. Force-induced fibronectin assembly and matrix remodeling in a 3D microtissue model of tissue morphogenesis. Integr. Biol. (Camb.) 4, 1164–1174.
Lemmon, C.A., Ohashi, T., Erickson, H.P., 2011. Probing the folded state of fibronectin type III domains in stretched fibrils by measuring buried cysteine accessibility. J. Biol. Chem. 286, 26375–26382.
Little, W.C., Smith, M.L., Ebneter, U., Vogel, V., 2008. Assay to mechanically tune and optically probe fibrillar fibronectin conformations from fully relaxed to breakage. Matrix Biol. 27, 451–461.
Little, W.C., Schwartlander, R., Smith, M.L., Gourdon, D., Vogel, V., 2009. Stretched extracellular matrix proteins turn fouling and are functionally rescued by the chaperones albumin and casein. Nano Lett. 9, 4158–4167.
Mao, Y., Schwarzbauer, J.E., 2005. Fibronectin fibrillogenesis, a cell-mediated matrix assembly process. Matrix Biol. 24, 389–399.
Montesano, R., Orci, L., 1988. Transforming growth factor beta stimulates collagen-matrix contraction by fibroblasts: implications for wound healing. Proc. Natl. Acad. Sci. U. S. A. 85, 4894–4897.
Murphy, G., Nagase, H., 2011. Localizing matrix metalloproteinase activities in the pericellular environment. FEBS J. 278, 2–15.
Nguyen, T.D., Liang, R., Woo, S.L., Burton, S.D., Wu, C., Almarza, A., Sacks, M.S., Abramowitch, S., 2009. Effects of cell seeding and cyclic stretch on the fiber remodeling in an extracellular matrix-derived bioscaffold. Tissue Eng. A 15, 957–963.
Overall, C.M., 2002. Molecular determinants of metalloproteinase substrate specificity: matrix metalloproteinase substrate binding domains, modules, and exosites. Mol Biotechnol. 22 (1), 51–86.
Pal, S., Chen, Z., Xu, X., Mikhailova, M., Steffensen, B., 2010. Co-purified gelatinases alter the stability and biological activities of human plasma fibronectin preparations. J. Periodontal Res. 45, 292–295.
Pankov, R., Yamada, K.M., 2002. Fibronectin at a glance. J. Cell Sci. 115, 3861–3863.
Pankov, R., Cukierman, E., Katz, B.Z., Matsumoto, K., Lin, D.C., Lin, S., Hahn, C., Yamada, K. M., 2000. Integrin dynamics and matrix assembly: tensin-dependent translocation of alpha(5)beta(1) integrins promotes early fibronectin fibrillogenesis. J. Cell Biol. 148, 1075–1090.
Parsons, M., Kessler, E., Laurent, G.J., Brown, R.A., Bishop, J.E., 1999. Mechanical load enhances procollagen processing in dermal fibroblasts by regulating levels of procollagen C-proteinase. Exp. Cell Res. 252, 319–331.
Prajapati, R.T., Chavally-Mis, B., Herbage, D., Eastwood, M., Brown, R.A., 2000. Mechanical loading regulates protease production by fibroblasts in three-dimensional collagen substrates. Wound Repair Regen. 8, 226–237.
Reinke, J.M., Sorg, H., 2012. Wound repair and regeneration. Eur. Surg. Res. 49, 35–43.
Romanic, A.M., Harrison, S.M., Bao, W., Burns-Kurtis, C.L., Pickering, S., Gu, J., Grau, E., Mao, J., Sathe, G.M., Ohlstein, E.H., Yue, T.L., 2002. Myocardial protection from ischemia/reperfusion injury by targeted deletion of matrix metalloproteinase-9. Cardiovasc. Res. 54, 549–558.
Ruangpanit, N., Chan, D., Holmbeck, K., Birkedal-Hansen, H., Polarek, J., Yang, C., Bateman, J.F., Thompson, E.W., 2001. Gelatinase A (MMP-2) activation by skin fibroblasts: dependence on MT1-MMP expression and fibrillar collagen form. Matrix Biol. 20, 193–203.
Seong, J., Tajik, A., Sun, J., Guan, J.L., Humphries, M.J., Craig, S.E., Shekaran, A., Garcia, A.J., Lu, S., Lin, M.Z., Wang, N., Wang, Y., 2013. Distinct biophysical mechanisms of focal adhesion kinase mechanoactivation by different extracellular matrix proteins. Proc. Natl. Acad. Sci. U. S. A. 110, 19372–19377.
Shaw, T.J., Martin, P., 2009. Wound repair at a glance. J. Cell Sci. 122, 3209–3213.
Shelton, L., Rada, J.S., 2007. Effects of cyclic mechanical stretch on extracellular matrix synthesis by human scleral fibroblasts. Exp. Eye Res. 84, 314–322.
Smith, M.L., Gourdon, D., Little, W.C., Kubow, K.E., Eguiluz, R.A., Luna-Morris, S., Vogel, V., 2007. Force-induced unfolding of fibronectin in the extracellular matrix of living cells. PLoS Biol. 5, e268.
Sohail, A., Sun, Q., Zhao, H., Bernardo, M.M., Cho, J.A., Fridman, R., 2008. MT4-(MMP17) and MT6-MMP (MMP25), A unique set of membrane-anchored matrix metalloproteinases: properties and expression in cancer. Cancer Metastasis Rev. 27, 289–302.
Sottile, J., Shi, F., Rublyevska, I., Chiang, H.Y., Lust, J., Chandler, J., 2007. Fibronectin-dependent collagen I deposition modulates the cell response to fibronectin. Am. J. Physiol. Cell Physiol. 293, C1934–C1946.
Soucy, P.A., Romer, L.H., 2009. Endothelial cell adhesion, signaling, and morphogenesis in fibroblast-derived matrix. Matrix Biol. 28, 273–283.
Speziale, P., Visai, L., Rindi, S., Di, P.A., 2008. Purification of human plasma fibronectin using immobilized gelatin and Arg affinity chromatography. Nat. Protoc. 3, 525–533.
Tomasek, J.J., Gabbiani, G., Hinz, B., Chaponnier, C., Brown, R.A., 2002. Myofibroblasts and mechano-regulation of connective tissue remodelling. Nat. Rev. Mol. Cell Biol. 3, 349–363.
Toriseva, M., Kahari, V.M., 2009. Proteinases in cutaneous wound healing. Cell. Mol. Life Sci. 66, 203–224.
Trelstad, R.L., Birk, D.E., 1985. The fibroblast in morphogenesis and fibrosis: cell topography and surface-related functions. Ciba Found. Symp. 114, 4–19.
Vihinen, P., Ala-aho, R., Kahari, V.M., 2005. Matrix metalloproteinases as therapeutic targets in cancer. Curr. Cancer Drug Targets 5, 203–220.
Visse, R., Nagase, H., 2003. Matrix metalloproteinases and tissue inhibitors of metalloproteinases: structure, function, and biochemistry. Circ. Res. 92, 827–839.
Vogel, V., 2006. Mechanotransduction involving multimodular proteins: converting force into biochemical signals. Annu. Rev. Biophys. Biomol. Struct. 35, 459–488.
Wang, Y.N., Sanders, J.E., 2003. How does skin adapt to repetitive mechanical stress to become load tolerant? Med. Hypotheses 61, 29–35.
Werner, S., Grose, R., 2003. Regulation of wound healing by growth factors and cytokines. Physiol. Rev. 83, 835–870.
Wilkinson, J.M., Davidson, R.K., Swingler, T.E., Jones, E.R., Corps, A.N., Johnston, P., Riley, G. P., Chojnowski, A.J., Clark, I.M., 2012. MMP-14 and MMP-2 are key metalloproteases in Dupuytren's disease fibroblast-mediated contraction. Biochim. Biophys. Acta 1822, 897–905.
Wong, V.W., Akaishi, S., Longaker, M.T., Gurtner, G.C., 2011. Pushing back: wound mechanotransduction in repair and regeneration. J. Investig. Dermatol. 131, 2186–2196.
Wong, V.W., Longaker, M.T., Gurtner, G.C., 2012. Soft tissue mechanotransduction in wound healing and fibrosis. Semin. Cell Dev. Biol. 23, 981–986.
Yang, C.M., Chien, C.S., Yao, C.C., Hsiao, L.D., Huang, Y.C., Wu, C.B., 2004. Mechanical strain induces collagenase-3 (MMP-13) expression in MC3T3-E1 osteoblastic cells. J. Biol. Chem. 279, 22158–22165.
Zamilpa, R., Lopez, E.F., Chiao, Y.A., Dai, Q., Escobar, G.P., Hakala, K., Weintraub, S.T., Lindsey, M.L., 2010. Proteomic analysis identifies in vivo candidate matrix metalloproteinase-9 substrates in the left ventricle post-myocardial infarction. Proteomics 10, 2214–2223.
Zhong, C., Chrzanowska-Wodnicka, M., Brown, J., Shaub, A., Belkin, A.M., Burridge, K., 1998. Rho-mediated contractility exposes a cryptic site in fibronectin and induces fibronectin matrix assembly. J. Cell Biol. 141, 539–551.